Nationaal Lucht- en Ruimtevaartlaboratorium
National Aerospace Laboratory NLR

NLR TP 96193

Experiences with ultra-high-bypass simulators from calibration and isolated engine testing

G.H. Hegen and R. Kiock

DOCUMENT CONTROL SHEET

	ORIGINATOR'S REF.		SECURITY CLASS.
	NLR TP 96193 U		**Unclassified**

ORIGINATOR
National Aerospace Laboratory NLR, Amsterdam, The Netherlands

TITLE
Experiences with ultra-high-bypass simulators from calibration and isolated engine testing

PRESENTED AT
Workshop on Aspects of Airframe Engine Integration for Transport Aircraft, 6-7 March 1996 in Braunschweig, Germany

AUTHORS	DATE	pp	ref
G.H. Hegen, R. Kiock	**960318**	**37**	**14**

DESCRIPTORS

Calibrating	**Prop-fan technology**
Engine airframe integration	**Simulators**
Engine tests	**Test facilities**
Engine inlets	**Turbofan engines**
Interference drag	**Wind tunnel models**

ABSTRACT
Investigations were carried out within a DLR/DNW/NLR co-operation on two Ultra High Bypass Ratio engine simulators. These so-called CRUF (Counter Rotating Ultra-high-bypass Fan) simulators were tested in isolation at low speed (July 1994) in the German Dutch Wind Tunnel (DNW) at the so-called Single Engine Support Stand (SESS). The CRUF calibrations, needed for thrust bookkeeping, were carried out in the NLR model Engine Calibration Facility (ECF, November 1994).
The average fan pressures of both CRUF units agree fairly well for the SESS and ECF tests. Both CRUF units show a rather large nacelle and pylon drag and a drag increase with increasing engine thrust. The prevention of ice build-up at core cowling and rake via a hot film at the outer core cowl surface worked properly and is strongly recommended for proper thrust bookkeeping.

Summary

Investigations were carried out within a DLR/DNW/NLR co-operation on two Ultra High Bypass Ratio engine simulators. These so-called CRUF (Counter Rotating Ultra-high-bypass Fan) simulators were tested in isolation at low speed (July 1994) in the German Dutch Wind Tunnel (DNW) at the so-called Single Engine Support Stand (SESS). The CRUF calibrations, needed for thrust bookkeeping, were carried out in the NLR model Engine Calibration Facility (ECF, November 1994).

The average fan pressures of both CRUF units agree fairly well for the SESS and ECF tests. Both CRUF units show a rather large nacelle and pylon drag and a drag increase with increasing engine thrust. The prevention of ice build-up at core cowling and rake via a hot film at the outer core cowl surface worked properly and is strongly recommended for proper thrust bookkeeping.

Contents

Nomenclature

A	area
A_W	wing area of ALVAST full span model (= 1.266 m^2)
C_D	drag coefficient (full span model or nacelle + pylon) (= $D/(q_\infty A_W)$)
C_{Do}	shape drag coefficient
C_L	lift coefficient (full span model or nacelle + pylon) (= $L/(q_\infty A_W)$)
C_p	pressure coefficient (= $(p - p_\infty)/q_\infty$)
Cd_c	core nozzle discharge coefficient (= $\dot{m}_5/\dot{m}_{5id}$ or $\dot{m}_8/\dot{m}_{8id}$)
Cd_f	fan nozzle discharge coefficient (= $\dot{m}_{15}/\dot{m}_{15id}$)
Cv_c	core nozzle velocity coefficient (= 1)
Cv_f	fan nozzle velocity coefficient (= $(F_{x,bal} - Cv_c\ \dot{m}_{5,8}\ Vj_{5,8})/(\dot{m}_{15}\ Vj_{15})$)
C_f	friction coefficient of flat plate
F_{bal}	balance force (wind tunnel or engine calibration facility)
FNPR	fan nozzle pressure ratio (= $\bar{p}_{t15}/p_\infty$)
$\dot{m}$	mass flow
Ma	Mach number
N	rotational speed
p	static pressure
p_t	total pressure
q	dynamic pressure ($q_\infty = 0.5\gamma p_\infty Ma_\infty^2$)
Re	Reynolds number based on pylon or nacelle length
R, r	radius
RPM	rotational speed
V	velocity
Vj	fully expanded (to p_∞) jet velocity
x	local coordinate along nacelle chord
α	angle of attack
γ	ratio of specific heats (= 1.4)
ε	thrust angle
λ	shape coefficient
φ	azimuth angle

Subscripts

∞	far upstream of model (windtunnel) or far downstream of model (calibration)
5	ahead throttle plate
8	behind throttle plate in the core exit plane

15	behind fan
id	ideal
isa	referred to ISA standard conditions
N	nacelle
P	pylon
W	wing

1 Introduction

For the next generation of engine families further reductions in fuel consumption and emissions are required. Therefore the development of the current high bypass turbofan engines follows a trend of new engine families with increasing bypass ratios. Improved efficiencies can be noted for these new engine types themselves but they also lead to larger engine fan diameters. Larger wetted nacelle areas with higher friction drag can be expected and the larger jet diameters will have stronger effects on engine-airframe integration. This contains the risk that the gains in fuel reduction are partly lost due to negative engine-airframe interference effects.

The integration of airframe and engines can be effectively investigated in wind tunnels using engine simulators. Both the DLR and NLR participated in the BRITE/EURAM program DUPRIN (DUcted PRopfan INvestigations). Within this framework the interference effects of Ultra High Bypass Ratio (UHBR) engines were experimentally determined at low speed in the DNW (German-Dutch Wind Tunnel). The DLR wind tunnel model ALVAST, two turbo-powered CRUF simulators (Counter Rotating Ultra-high-bypass Fan) and two conventional turbo-powered simulators were used. The test results with the CRUF simulators showed a remarkable increase in total drag compared to the conventional turbofan simulators [1]. Besides a non-linear drag behaviour with engine rotational speed can be noted for both types of simulators (see Fig. 1 [2]).

For a better understanding of the interference effects mentioned above, further investigations were needed. These investigations were carried out within a DLR/DNW/NLR co-operation outside of the DUPRIN framework and limited to the CRUF simulators. The CRUF units were tested in isolation at low speed (July 1994) in the German Dutch Wind Tunnel (DNW) at the so-called Single Engine Support Stand (SESS). Both CRUF simulators have been tested because the simulators differ slightly in instrumentation and turbine layout. The SESS measurements should indicate the drag and lift forces of the isolated simulator including the pylon.

To find the drag and lift of the simulator, the simulator gross thrust and ram drag force (intake mass flow times wind tunnel velocity) should be subtracted from the forces measured by the balance during the wind tunnel test. For proper wind tunnel thrust and drag force bookkeeping it is necessary to know these values with very high accuracy. The CRUF units are supplied with instrumentation in the fan and core duct to calculate ideal mass flow and thrust. In the DUPRIN I and II program the relation with the actual mass flow and gross thrust was determined in the NLR model Engine Calibration Facility (ECF).

The SESS results were analysed and reported for the first time in [3]. At that time only DUPRIN I calibrations of the CRUF units (November 1992) were available [4], which were in fact not

applicable for all cases. Suitable CRUF calibration data became available in the DUPRIN II program [5] (November 1994), and were used for a renewed analysis of the SESS results [6], to be described in this paper.

2 Engine models

The UHBR simulator is based on the concept of the Counter Rotating Integrated Shrouded Propfan (CRISP) of MTU München, see [7]. H. Hoheisel [8] specified this new UHBR simulator and named it Counter Rotating Ultra-High-Bypass Fan (CRUF) simulator. CRUF I (Fig. 2) was designed in cooperation between DLR and Dynamic Engineering Inc. (DEI) [9], Newport News, VA, and was manufactured by DEI. Each fan rotor has eight blades designed by MTU, München, and made of carbon fibre composites by NLR. The asymmetric nacelle was designed by DLR [10] and was used during the DUPRIN I program on the ALVAST model in cruise configuration. Nacelle and pylon were manufactured by DLR. A second UHBR unit - CRUF II - was manufactured within DUPRIN I by Technofan, Toulouse and based on the same specification as for CRUF I.

Some main parameters of both CRUF units are described in table 1. The fan diameter is 254 mm (10"). Pressurized air drives a four-stage turbine which is connected to the counter-rotating fan via a reversal gear. Unfortunately, the turbine is not able to expand the air down to ambient conditions, because core geometry and the ratio of core thrust to fan net thrust had to be as close as possible to CRISP [8]. Therefore, a throttle plate was installed in the core duct downstream of the turbine. Since the two CRUF units were manufactured by different firms, the turbine design differs slightly and the throttle plate geometry, too. These plates have circular holes of 4.9 to 10.5 mm diameter (CRUF I, solidity 0.549) and of 7.0 to 10.5 mm diameter (CRUF II, solidity 0.436).

The instrumentation is sketched in figure 3. Initially it was intended to have the instrumentation of both CRUF units identical, but for different reasons this was not possible. The fan duct instrumentation in plane 15 (see Fig. 2) consists of:

- CRUF I : 3 rakes with 5 pitot probes each, 4 thermocouples, 2 PT100 temperature sensors.
- CRUF II : 5 rakes with 5 pitot tubes each,5 PT100 temperature sensors.

The core instrumentation in plane 5 (upstream of throttle plate) and plane 8 (downstream of throttle plate in core exit plane) consists of:

- CRUF I, plane 5 : 6 pitot probes, 2 thermocouples.
  plane 8 : 3 rakes with 5 pitot probes each, 4 PT100 temperature sensors.
- CRUF II, plane 8 : same as CRUF I.

Initial tests showed icing of the fan jet flow on the core cowls of both CRUF units near the nozzle exit due to the low temperature at the core exit (200K at RPM = 14500 rev/min). Therefore, thin heated films were mounted first on the outer core cowl surface of CRUF I and a temperature of 50 ± 1°C was maintained at rotational speeds above RPM = 6000 rev/min. When heating is applied, nearly no ice is observed up to RPM = 13500 rev/min for both calibration and wind tunnel test. Due to the success of heating, also CRUF II was equipped with heating films after the SESS tests and before the ECF calibration.

In addition, the fan cowl of CRUF II is equipped with surface pressure taps in three sections at φ = 60°, 180° and 300° with 20 taps each. Transition is forced on the outer nacelle surface at 10% of the local nacelle chord length by carborundum 70K (size 0.25 mm).

3 Experimental set-up

3.1 Model Engine Calibration Facility

The main part of the NLR Model Engine Calibration Facility (ECF) (see Fig. 4) is a vacuum tank, having a diameter of 3 m and a length of 6 m. In the ECF the thrust vector and mass flows of a model engine are determined under simulated wind tunnel conditions without external flow. The model engine is mounted in the front end of the test tank. The engine inlet is open to ambient atmospheric conditions and the nozzles exhaust into the tank. The wind tunnel ram pressure ratio is simulated statically by setting an appropriate pressure difference between inlet and exhaust environment. This condition is established by vacuum pumps which evacuate the tank. For more information, see [5].

3.2 Single Engine Support Stand at DNW

The CRUF simulators were tested in the 8m x 6m test section of the German-Dutch Wind Tunnel (DNW) [11] on the Single Engine Support Stand (SESS) which has an aerodynamic shape as shown in figure 5. The SESS has been designed for a uniform velocity field in the volume where simulator plus pylon are to be mounted. The simulator is connected to a six-component balance inside the SESS body, which measures forces and moments acting on simulator and pylon. This balance has an absolute accuracy of ±3.25 N and a reproducibility of ±1.1 N, both in its axial X-direction. Pressurized air is dried to a dew point of at least 200K at 1 bar and feeds the simulator via air bridges and the original pylon. The simulator axis is adjusted parallel to the SESS axis. The data evaluation was described in [12].

4 ECF test program

Prior to the CRUF calibration itself the measurement chain was validated by carrying out a number of pretest calibrations and checks (according to standard practice, see [5]). In this way the stability and behaviour of both CRUF systems (for instance health monitoring) were verified over their entire operating envelope. The CRUF I engine rotational speed was limited to 13500 rev/min instead of the specified maximum of 15400 rev/min to respect the maximum bearing temperature limit. The CRUF II simulator could be run to the specified maximum RPM = 15600 rev/min without any problems in view of bearing temperatures.

For the two CRUF units the relation between actual mass flows and gross thrust, and the ideal values from engine instrumentation were determined in the ECF. These relations are defined via the core discharge coefficient Cd_c, fan discharge coefficient Cd_f, fan velocity coefficient Cv_f (assuming $Cv_c = 1$) and thrust angle ε. The calibrations were performed for Ma_∞ = 0.18, 0.22, 0.25 and 0.27. Data points were collected at a sequence of RPM settings, which were selected after the function check. Repeat data points are collected to show repeatability within the run. Before the actual CRUF calibration measurements, the CRUF and the ECF were given some time (approximately 5 minutes) to achieve thermal equilibrium at an RPM of about 6000 rev/min. For CRUF I calibrations were carried out with and without heating of the core cowl.

5 DNW test program

Both CRUF units were investigated in a range of Mach number from Ma_∞ = 0.18 to 0.25, angle of attack for α = 0° and 6° and rotational speed from RPM = 3800 to 15000 rev/min. The balance data were corrected for the residual forces (introduced by pressures and temperatures) of the airbridge system. Balance forces, engine gross thrust and ram drag result in CRUF drag and lift coefficients (which are defined on A_W = 1.266 m^2, the wing area of ALVAST full scale model), as described in [3]. The drag coefficient $C_{D,N+P}$ of nacelle and pylon is required for the evaluation of the interference drag ΔC_D of the full scale model equipped with two engines:

$$\Delta C_D = C_{D,model} - C_{D,wings+fuselage} - 2C_{D,N+P}$$

Rotational speed, forces and mass flow were transferred to isa standard conditions [3].

6 Test results

6.1 ECF results

In figures 6 and 7 some typical calibration results of the CRUF I unit with hot film on and off, and the CRUF II unit (no heating available) are shown. Besides, the CRUF I data are presented using one time the core duct rake behind the throttle plate (plane 8) and the other time using the core duct rake ahead of the throttle plate (plane 5) for data processing. The fan pressure distributions are symmetrical to the vertical axis (see section 6.2.1) and since the fan geometries including the blading of CRUF I and II are identical, it was decided for the data processing to mirror the pressures of fan rake 2 and 3 of CRUF I resulting in extra rakes 2a and 3a. In this way the (fictitious) CRUF I fan rake geometry becomes identical to the CRUF II fan rakes (see Fig. 3).

The calibration coefficients Cd_f and Cv_f measured at Mach number $Ma_\infty = 0.22$ are presented as a function of Fan Nozzle Pressure Ratio (FNPR). The repeatability of the Cd_f and Cv_f is of the order of ±0.15% and ±0.25% respectively (95% confidence level) at moderate and high power settings for both CRUF units. The Cv_f coefficient of the CRUF I unit shows to be strongly dependent on FNPR when the core duct rake ahead of the throttle plate is used. This is considered to be the consequence of assuming $Cv_c = 1$ (usually at TPS calibration no losses are assumed from the rake station to the nozzle exit plane). The higher total pressure at plane 5 (compared to plane 8) results in much higher values for the calculated ideal core mass flow and ideal core velocity. This results in significantly lower Cv_{f5} values.

The Cd_f coefficients of both CRUF units are quite similar and differ only by 1%. These magnitudes can be expected from differing model and fan rake hardware. The differences in the Cv_f and Cd_c (not shown here) coefficients are higher, even when both units are processed with the core duct rake behind the throttle plate. These are caused by the different layouts of turbines and throttle plates. The average value of the measured total pressure behind the throttle plate has some uncertainty because some of the total pressure probes are located in an area with little or no flow due to blockage of the throttle plate. This explains for CRUF II the large Cv_f coefficient (close to and higher than 1).

As may be expected the Cd_f coefficient of the CRUF I unit is not affected by the prevention of ice accretion on the core nozzle. But systematical differences and repeatability improvements at the higher power settings can be noted for the $Cd_{c5,8}$ coefficient and for the $Cv_{f5,8}$ coefficient, when the heating film is switched on.

The repeatability in vertical thrust angle ε is good and is about ±0.15° at high FNPR. A mean

value of 0.8° is estimated for both CRUF units independent of Mach number.

6.2 Analysis of DNW results

Windtunnel results will be primarily discussed for $Ma_\infty = 0.22$ and $\alpha = 0°$. Heating of the core cowl is not applied unless specified otherwise.

6.2.1 Fan pressure

The local pressure ratio p_{t15}/p_∞ behind the fan of CRUF II was plotted versus radius R in figure 8. All rakes show a total pressure profile similar to that one of the design [8]. The total pressure level of rake 1 is higher than at the other rakes because of the flow throttling by the wider pylon strut which is 35 mm in comparison with 10 mm width of the other 4 struts containing rakes 2 to 5. This throttling may cause that the fan operates locally at different performance conditions. This can be also stated at rakes 2 and 5 which are neighboured to rake 1. The very similar pressure distributions of rakes 2 and 5 on one side and of rake 3 and 4 on the other side indicate the symmetrical behaviour of the fan flow of CRUF II.

Figure 8 shows also a comparison with the ECF results. The latter were interpolated for RPM to get agreement with the rotational speed RPM of the windtunnel tests. At high RPM the results differ slightly (higher fan exit pressures in wind tunnel) because in the windtunnel, an asymmetric intake was used, while an axisymmetric bellmouth and an axisymmetric intake were applied during calibration. Since the inlet mass flow ratio (stream tube contraction) is determined by the rotational speed, it is expected that the fan operation is influenced by the intake condition. Further, during calibration there is no external flow around the fan cowl and therefore another pressure field develops in the fan flow nozzle exit area.

Figure 9 shows the results of CRUF I. The agreement of windtunnel and calibration data is similar and again the windtunnel fan pressure is in general a little higher than during calibration.

The average pressure expressed as fan nozzle pressure ratio FNPR is shown in figure 10. The results of calibration and wind tunnel agree fairly well, and also CRUF I and II are very close to each other. At $RPM_{isa} = 13306$ rev/min, the corrected fan mass flow of CRUF I lies only by 0.1 kg/s or 1.5% above that of CRUF II. Expressed as corrected fan gross thrust, the difference amounts only to 11 N or 1%. There is nearly no difference between $\alpha = 0°$ and 6°.

6.2.2 Core pressure

The local pressure ratio p_{t8}/p_∞ in the core nozzle exit of CRUF II is plotted in figure 11. The pressure distribution can be quite irregular because the total pressure is measured close behind the throttle plate. The 72 individual jets from this plate are mixing randomly downstream. Near hub and casing the local pressure p_{t8} even lies somewhat below p_∞. Hence, disagreement of

windtunnel and calibration data can be expected.

The resulting average total pressure ratio in plane 8 is shown in figure 12. Despite the throttle plate, the average values show very little spread when plotted as a function of RPM. In detail it can be stated:

- The pressure levels of CRUF I and II are different due to the different turbine design.
- The CRUF I data of the calibration clearly show the influence of heating. Due to the low ambient temperature in November, the fan air was cold and ice accretion started at about RPM_{isa} = 9000 rev/min causing certain blockage at higher RPM. This is not observed when heating is applied.
- The CRUF I data of the wind tunnel do not show this effect because of higher ambient temperature in July and corresponding negligible ice accretion (very similar behaviour was found in plane 5 which is not shown here).
- The disagreement between the CRUF II calibration and wind tunnel test are probably due to the mentioned irregular local pressure and ice accretion effects i.e. ice accretion during the calibration only.

6.2.3 Balance Force and Net Thrust

The axial force $F_{x,bal}$ measured on the balance in the windtunnel is shown in figure 13. This force consists of engine net thrust and of nacelle/pylon drag. For comparison, the net engine thrust is included here. CRUF I produces more thrust than CRUF II at the same rotational speed, i.e. 45 N more at RPM_{isa} = 13300 rev/min. In other words, CRUF II has to run by 370 rev/min faster in order to produce the same net thrust as CRUF I.

6.2.4 Drag

First the drag coefficient of CRUF I nacelle and pylon is shown in figure 14 based on the core data of plane 5 (upstream of throttle plate). The drag increases steadily with RPM. It amounts to C_D = 0.0018 at RPM_{isa} = 5530 rev/min and reaches C_D = 0.0038 at RPM_{isa} = 11700 rev/min at Ma_∞ = 0.22 (α = 0°, heating on). It is verified first whether the pure drag of nacelle and pylon can be as high as shown.

The shape drag $C_{Do,N+P}$ of nacelle outer surface and pylon was estimated on the basis of fully turbulent flow along a flat-plate including a shape coefficient λ to account for the local velocity being different from the free stream value, see [13]:

$$C_{Do,N+P} = C_{f,N}\frac{A_{wet,N}}{A_W}\lambda_N + C_{f,P}\frac{A_{wet,P}}{A_W}\lambda_P$$

with A_{wet} as wetted area, $C_f = 0.455/(\log Re)^{2.58}$ and with the wind tunnel speed ($Ma_\infty = 0.22$) and the characteristic length of nacelle or pylon in the Reynolds number calculation. For the pylon a value $\lambda_p = 1.33$ was chosen but for the nacelle λ_N will depend on the location of the stagnation point as determined by the intake mass flow ratio. Assuming a velocity distribution that varies linearly from a peak value at the nacelle lip to the free stream value at the fan nozzle exit, a shape factor $\lambda_N = 1.5$ was found for $C_p = -0.8$ at the lip (low RPM) decreasing to $\lambda_N = 1.1$ for $C_p = -0.2$ at the lip (maximum RPM). Hence $C_{Do,N+P}$ of the CRUF nacelle and pylon will decrease accordingly from $C_{Do,N+P} = 0.0014$ to $C_{Do,N+P} = 0.0011$. The shape drag of one engine/pylon in [13] amounts to $C_{Do,N+P} = 0.00085$ (using $\lambda_N = 1$) at low speed and also referred to the full model wing area. That is less than the value of CRUF, but it has to be considered that CRUF has bigger diameter and pylon length.

An example of nacelle/pylon installation drag is presented in [14] for high speed. The drag increments like nacelle vortex drag, nacelle lip drag, core cowl and stub scrubbing drag lead to a drag coefficient of 0.0026 which is by 1.6 above the pure shape drag at low lift. Applying this factor to CRUF we get 0.0022 at low RPM and 0.0018 at high RPM.

The measured drag level at low RPM corresponds with the estimations but the increase of C_D with increasing RPM and decreasing Mach number is opposite to common experience (see also above): the drag should decrease with increasing mass flow ratio because this leads to a more outward location of the stagnation point. Possibly the drag increase should not be attributed to an increase in external drag but to an increase in internal intake drag i.e. lower engine thrust. For mass flow ratios higher than 1, a suction peak develops on the inner lip contour and at maximum RPM local flow velocities above M = 0.65 are observed, corresponding to $C_p = -5$. This leads to an increase in internal intake drag of about $\Delta C_D = 0.0020$. The thicker internal intake boundary layer could hardly be observed by the total fan pressure probe nearest to the wall (minimum distance is about 5 mm). From the fan rake probes a thrust is predicted according to the ECF calibration but in fact the thrust may have decreased unnoticed by the rake. Static wind tunnel tests ($Ma_\infty = 0$) on the CRUF simulator with and without bellmouth would give more insight in the possible variation in internal intake drag.

Anyway, the apparent increase in aircraft drag with increasing RPM shown in figure 1 is therefore very likely dominated by a decrease in thrust of the simulator rather than by interference drag.

Heating has considerable influence: C_D falls down with no heating above RPM_{isa} = 10700 rev/min when considerable ice accretion was visible in the ECF (decrease in thrust) but not on the SESS. So the fall in drag is erroneously concluded from the calculated engine thrust, which is too low. The effect of α (0° and 6°) is small.

The alternative C_D evaluation again for CRUF I with plane 8 data is shown in figure 15. With heating the results of Figure 14 and 15 are very close (within the balance repeatability of ±5 drag counts) up to RPM_{isa} = 12200 rev/min but disagree for higher RPM. Without heating disagreement already exists above RPM_{isa} = 9000 rev/min.

Figure 16 shows corresponding data for CRUF II but C_D increases with angle of attack as is to be expected and in contrast with CRUF I.

Finally, interference of the SESS body cannot be excluded. The free area between SESS body and CRUF amounts only to one CRUF diameter (see Fig. 5).

6.2.6 Lift

The lift coefficient of CRUF I in figure 17 is negative at zero angle of attack due to the different nacelle profiles around the circumference. It amounts to C_L = -0.007 at α = 0° and increases to C_L = -0.004 at α = 6° (Ma_∞ = 0.22 and RPM_{isa} = 6000 rev/min). A maximum lift rise ΔC_L = 0.0030 with RPM (from RPM_{isa} = 6000 rev/min to RPM_{isa} = 13300 rev/min) was observed which would correspond to an increase in angle of attack of $\Delta\alpha$ = 0.03° for the ALVAST cruise configuration with CRUF. For CRUF II similar results (levels) can be noted.

7 Outlook

In the future, the UHB engine simulators will be incorporated in the DLR/NLR cooperation in order to investigate the wake of ALVAST wing/simulator by five-hole probe rake and particle-image velocimetry. One UHB simulator will be used during the evaluation of jet-engine interference at transonic speed on the ALVAST half model together with turbofan and VHBR simulator in the ENIFAIR program sponsored by BRITE/EURAM.

The drag is influenced by the inaccurate measurement of CRUF core pressure. The treatment of the throttle plate and of the core calibration coefficients Cd_c and Cv_c has to be investigated further.

8 Conclusions

The drag coefficient of two Counter Rotating Ultra-high-bypass Fan simulators was to be determined experimentally. The two CRUF units have the same fan geometry with 254 mm fan diameter and the same core nozzle exit diameter of 115 mm but slightly differing turbine design. Both CRUF units expand their core jets via a throttle plate to ambient conditions.

Calibration was carried out in the Engine Calibration Facility of NLR. The isolated CRUF units were tested one after the other on the Single Engine Support Stand in the 8m x 6m test section of DNW. The main results at $Ma_\infty = 0.22$ are summarized as follows:

- The fan nozzle pressure ratios of calibration and wind tunnel of each CRUF agree fairly well. The fan characteristics like fan nozzle pressure ratio, corrected fan mass flow and corrected fan gross thrust are in very good agreement for CRUF I and II.
- The local total pressure downstream of the throttle plate is somewhat uncertain due to random mixing of the individual jets of the throttle plate. In contrast, the average values form a smooth behaviour as a function of RPM but agreement between calibration and wind tunnel is observed for CRUF I only. Ice accretion on the core cowl at high RPM influences this pressure considerably. Heated films on the core cowl suppress icing effectively.
- The different design of turbine and throttle plate leads to higher core thrust of CRUF I.
- The drag coefficient of CRUF nacelle and pylon was estimated at $Ma_\infty = 0.22$ on the basis of a fully turbulent flow along a flat-plate including a shape coefficient for pylon and nacelle. Referred to a wing area of $A_W = 1.266\ m^2$, C_{Do} varies between 0.0014 and 0.0011 dependent on the RPM. Inclusion of further drag increments would lead to 60% higher values.
- This drag level was evaluated from the SESS tests on CRUF I. The measured drag level at low RPM corresponds with the estimations but, opposite to common experience and the estimations, it increases with mass flow ratio (higher RPM or lower Mach number) at both $\alpha = 0°$ and 6°. Possibly the drag increase should not be attributed to an increase in external drag but to an increase in internal intake drag i.e. lower engine thrust. Static wind tunnel tests ($Ma_\infty = 0$) on the CRUF simulator with and without bellmouth would give more insight in possible explanations.
- The apparent increase in aircraft drag with increasing RPM shown in figure 1 is very likely dominated by a decrease in thrust of the simulator rather than by interference drag.
- The drag of CRUF I and II differ to some extent due to different core situations.
- Heating of the core cowl is strongly recommended especially during calibration because icing distorts the pressure/temperature measurements behind the core cowl and results in drag which is too low.

- The nacelle lift coefficient at zero angle of attack is negative because of the different nacelle profiles around its circumference.

9 References

[1] Burgsmüller, W.; Hoheisel, H.; Kooi, J.W., *Engine/Airframe Interference on Transport Aircraft with Ducted Propfans - The European Research Programme DUPRIN -*, ICAS-94-3.7.1 (1994).

[2] Hoheisel, H., *Das Europäische Forschungsprogramm DUPRIN*, DLR-Nachrich-ten, Heft 76 (1994).

[3] Steeger, B., *Analyse von Untersuchungen an isolierten UHB-Triebwerkssimulatoren im Windkanal, Diplomarbeit Nr. 241 Institut für Strömungsmechanik, TU Braunschweig* , DLR-IB 129-95/1 (1995).

[4] Slauerhoff, J.F., *Calibration of two Counter Rotating Ultra-high-bypass Fan simulator units in the Model Engine Calibration Facility - test number 3905 -*, NLR CR93458L (1993).

[5] Hegen, G.H., *Re-calibration on two Counter Rotating Ultra-high-bypass Fan Simulator Units for DUPRIN II in the model Engine Calibration Facility - test numbers 4912 and 5903 -*, NLR CR95640L (1996).

[6] Kost, D., *Analyse von experimentellen Untersuchungen an isolierten UHB-Trieb-werkssimulatoren, Diplomarbeit FH Wolfenbüttel (1996).*

[7] Grieb, H.; Eckardt, D., *Propfan and Turbofan, Antagonism or Synthesis*, ICAS- 86-3.8.2 (1986).

[8] Hoheisel, H., *The Design of a Counter Rotating Ultra-high-Bypass Fan Simulator for Windtunnel Investigation*, DLR-FB 93-20 (1993).

[9] Hoheisel, H; Knap, M., *Development and Use of an Ultra-High-Bypass Ratio Engine Simulator*, International Forum on Turbine Powered Simulation, DNW, Emmeloord, The Netherlands (1995).

[10] Kiock, R.; Hoheisel, H., *Design of the Axi-Asymmetric Nacelle for the Counter Rotating Ultra-High-Bypass Fan Simulator*, DLR-FB 93-52 (1993).

[11] Kooi, J.W.; Kiock, R.; Slauerhoff, J.F., *Tools for the Experimental Study of the Integration of Ultra-High Bypass Engines on Transport Aircraft*, AIAA paper no. 94-2562 (1994).

[12] Eckert, D.; Van Ditshuizen, J.C.A.; Munniksma, B.; Burgsmüller, W., *Low Speed Twin Engine Simulation on a Large Scale Transport Aircraft Model in the DNW*, ICAS-84-2.10.4 (1984).

[13] Haftmann, B.; Debbeler, F.-J.; Gielen, H., *Takeoff Drag Prediction for Airbus A300-600 and A310 Compared with Flight Test Results*, J. Aircraft Vol. 25, No. 12 (1988).

[14] Harris, A.E.; Kutney, Snr., J.T.; Ogilvie, F.B., *25 years of Turbine Powered Simulation Success*, International Forum on Turbine Powered Simulation, DNW, Emmeloord, The Netherlands (1995).

10 Acknowledgement

The authors gratefully acknowledge the support of this contribution by J.W. Kooi and D. Ehlen of DNW, by H. Hoheisel of DLR, by W.B. de Wolf of NLR, by D. Hummel of TU Braunschweig as well as by B. Steeger and D. Kost. These names are mentioned to stand in place of many others of DNW, NLR and DLR who were participants in this work, too.

Table 1 Drag of ALVAST model with engine simulators, cruise geometry

Bypass ratio to be simulated	15.7
Fan pressure ratio	1.21
Fan nozzle exit Mach number	0.56
Fan mass flow, kg/s	7.2
Turbine mass flow, kg/s	1.5
Fan power requirement, kW	162
Turbine inlet pressure, bar	20
Wind tunnel Mach number	0.176
Rotational speed, RPM	16350

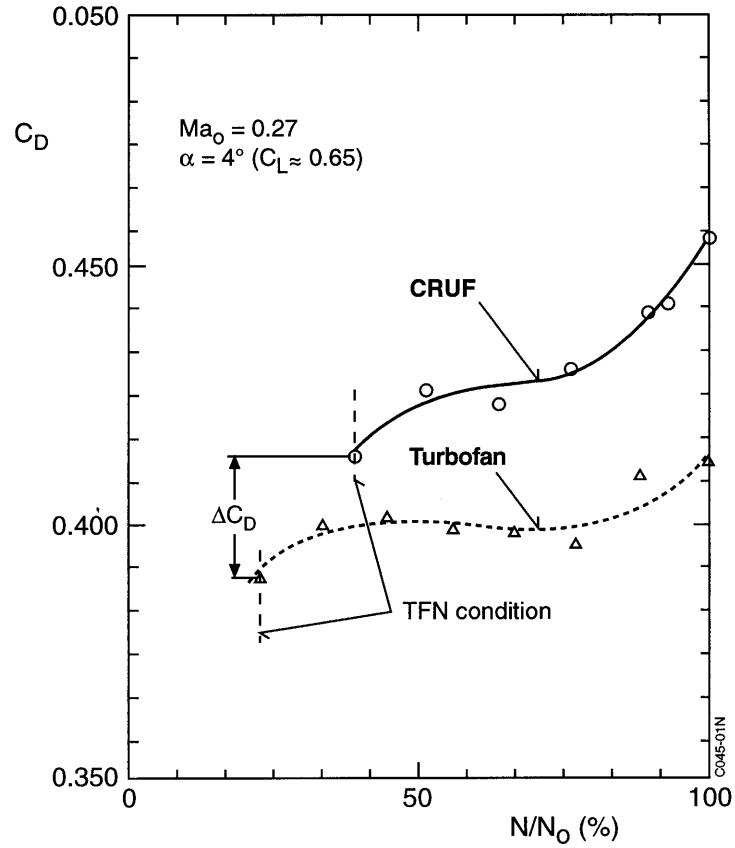

Fig. 1 Drag of ALVAST model with engine simulators, cruise geometry

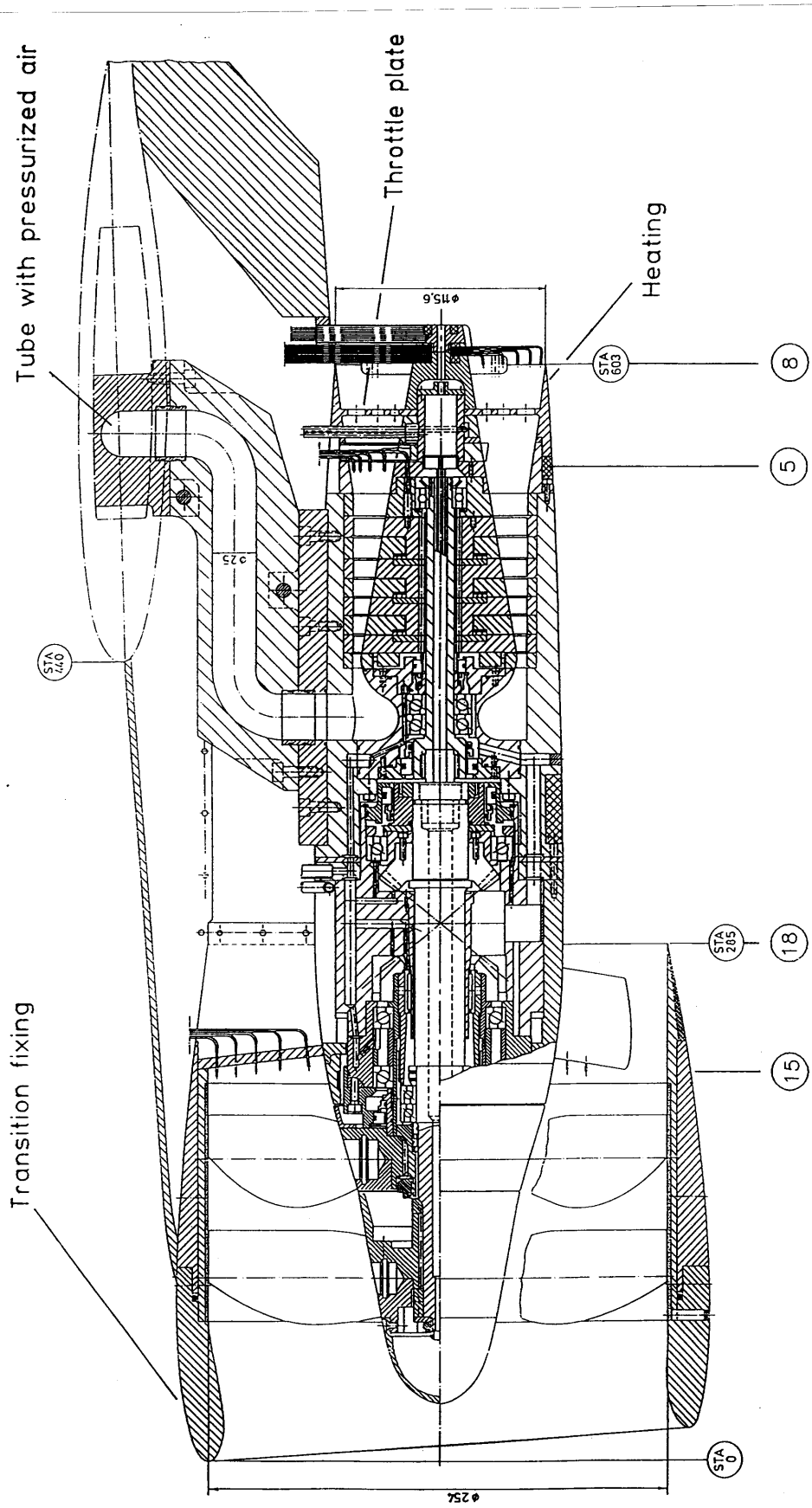

Fig. 2 UHBR engine simulator CRUF I

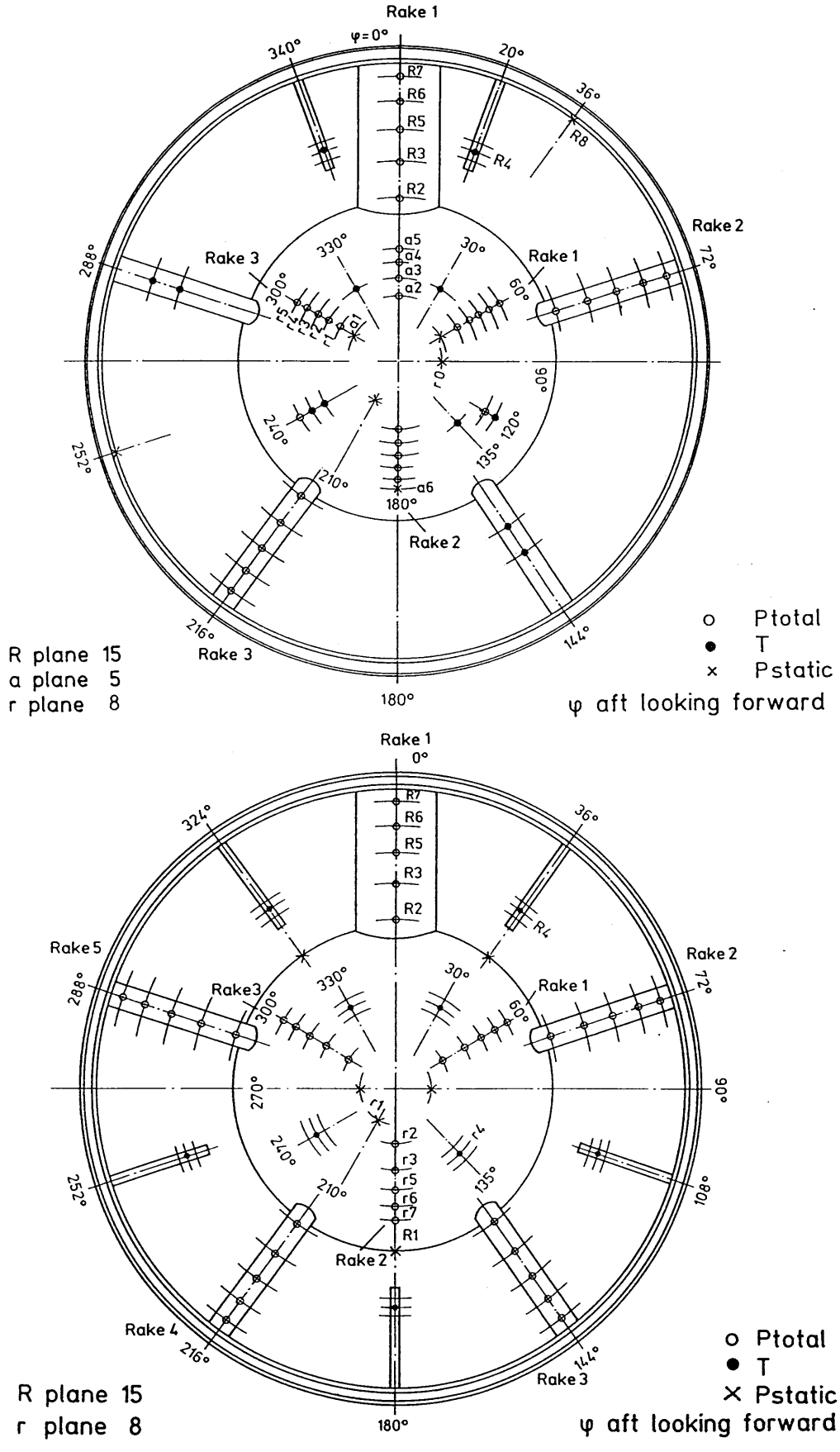

Fig. 3 Instrumentation on CRUF I (top) and CRUF II (bottom)

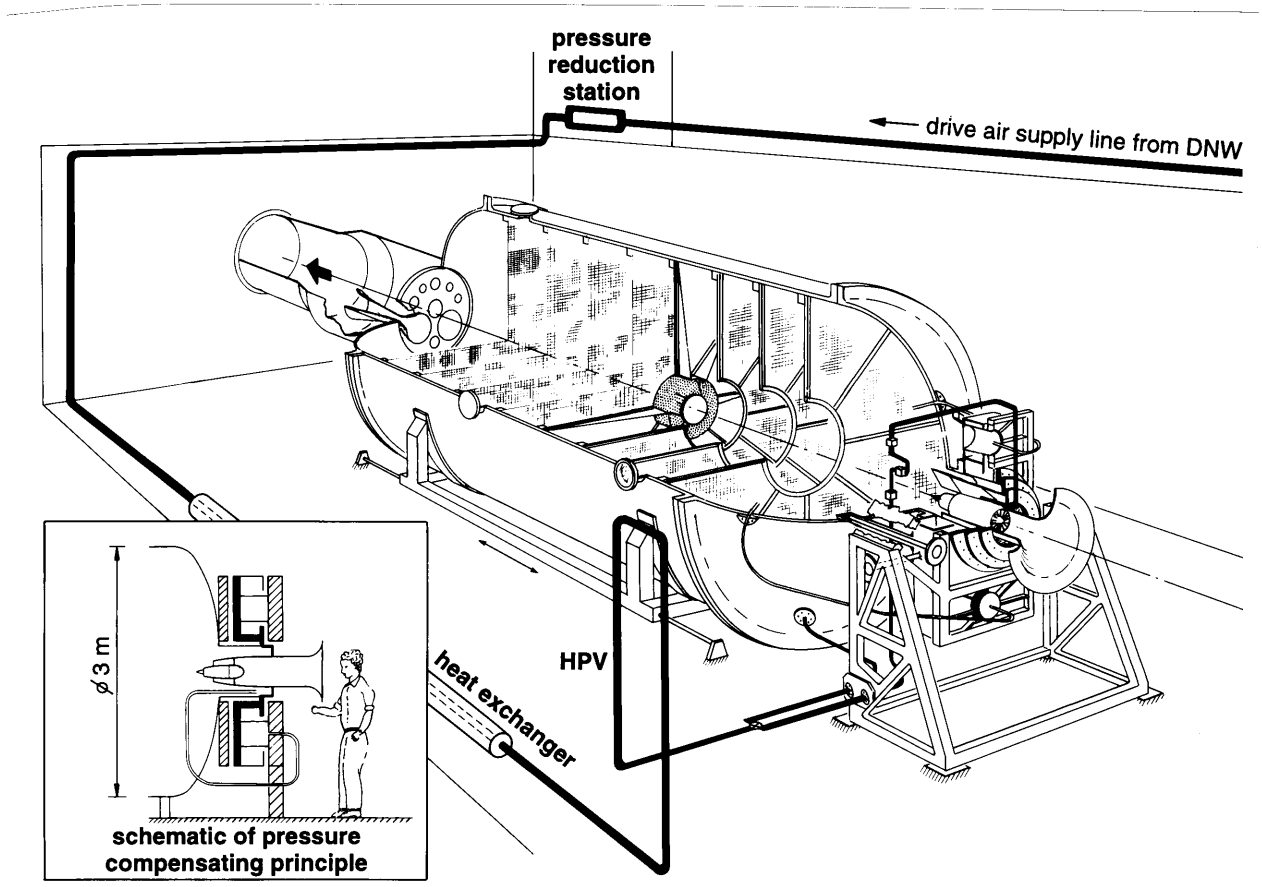

Fig. 4 Engine Calibration Facility (ECF)

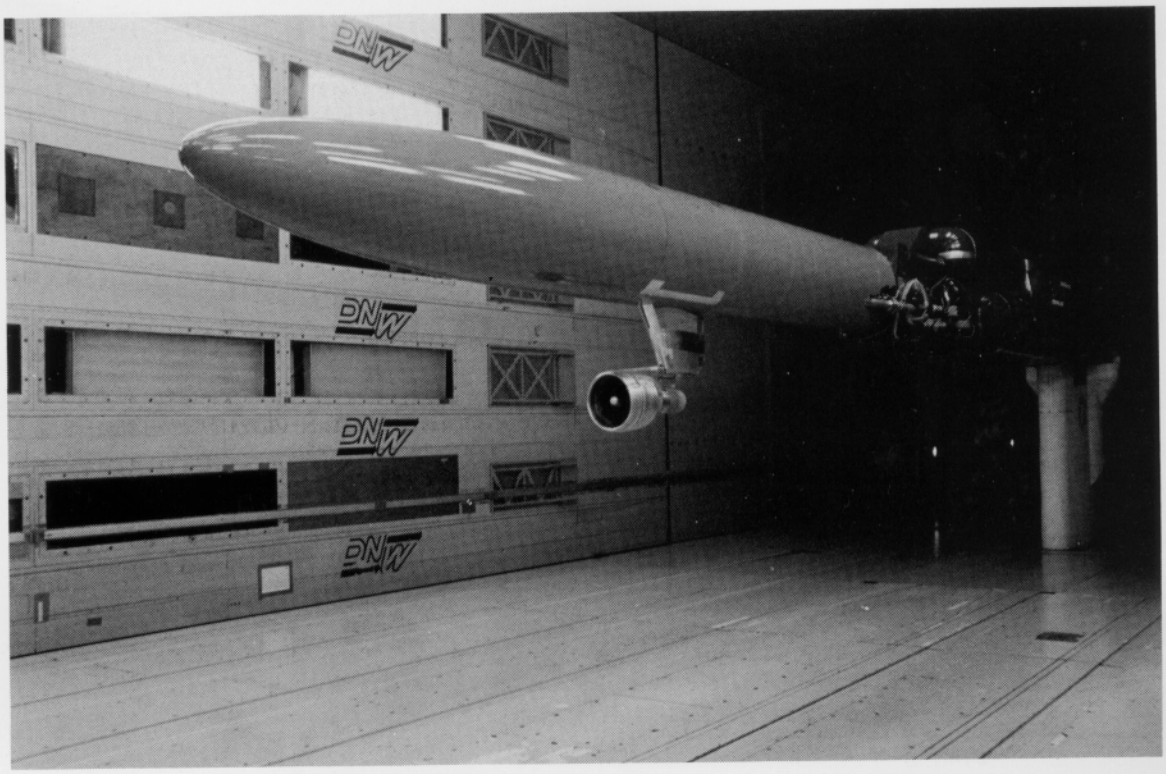

Fig. 5a View of SESS with CRUF

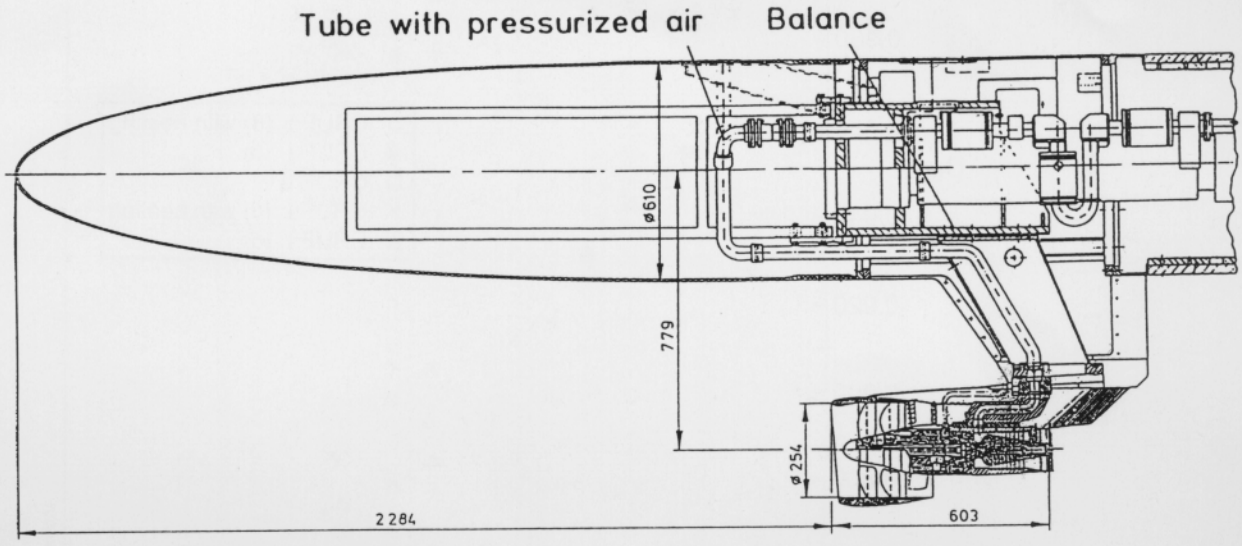

Fig. 5b Details of CRUF installation on SESS

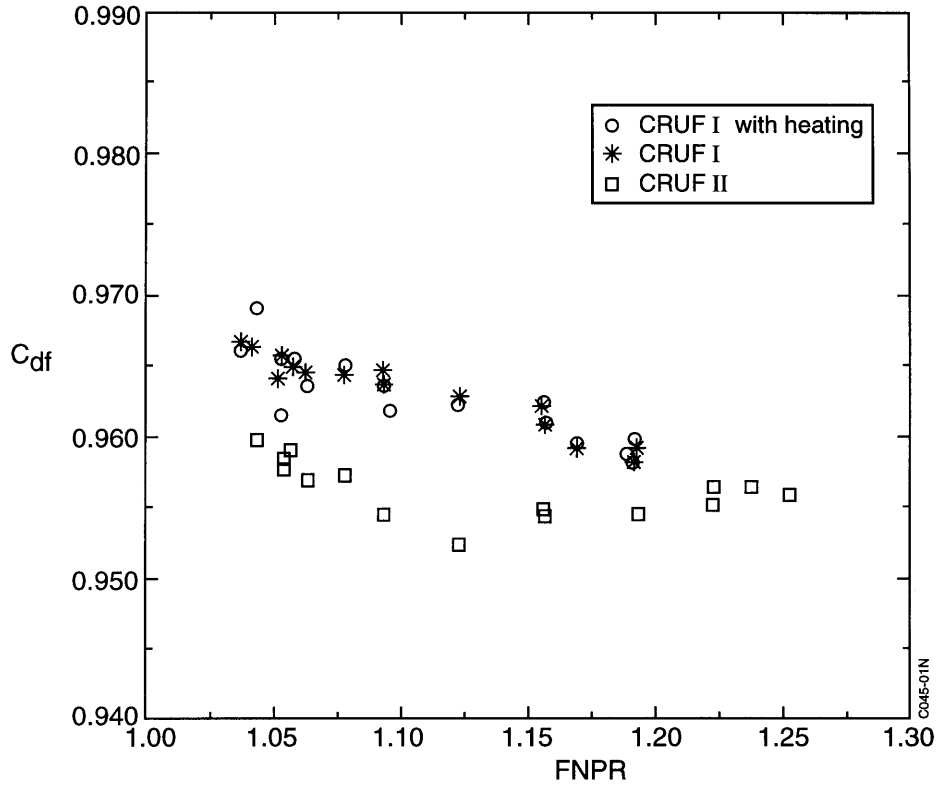

Fig. 6 Fan discharge coefficient

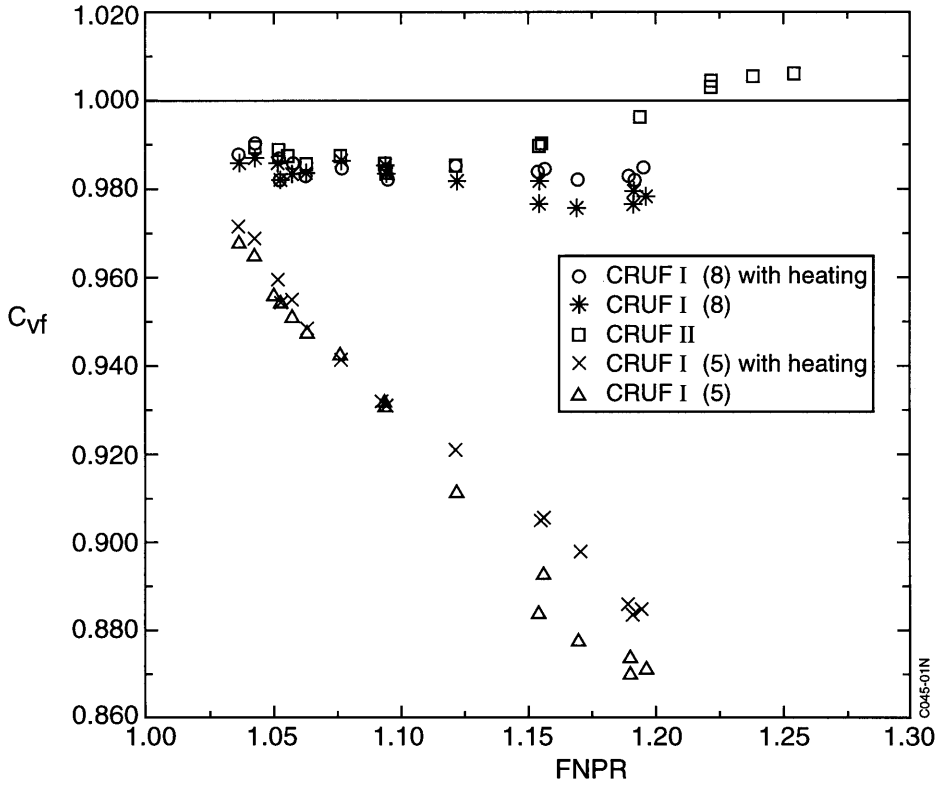

Fig. 7 Fan velocity coefficient

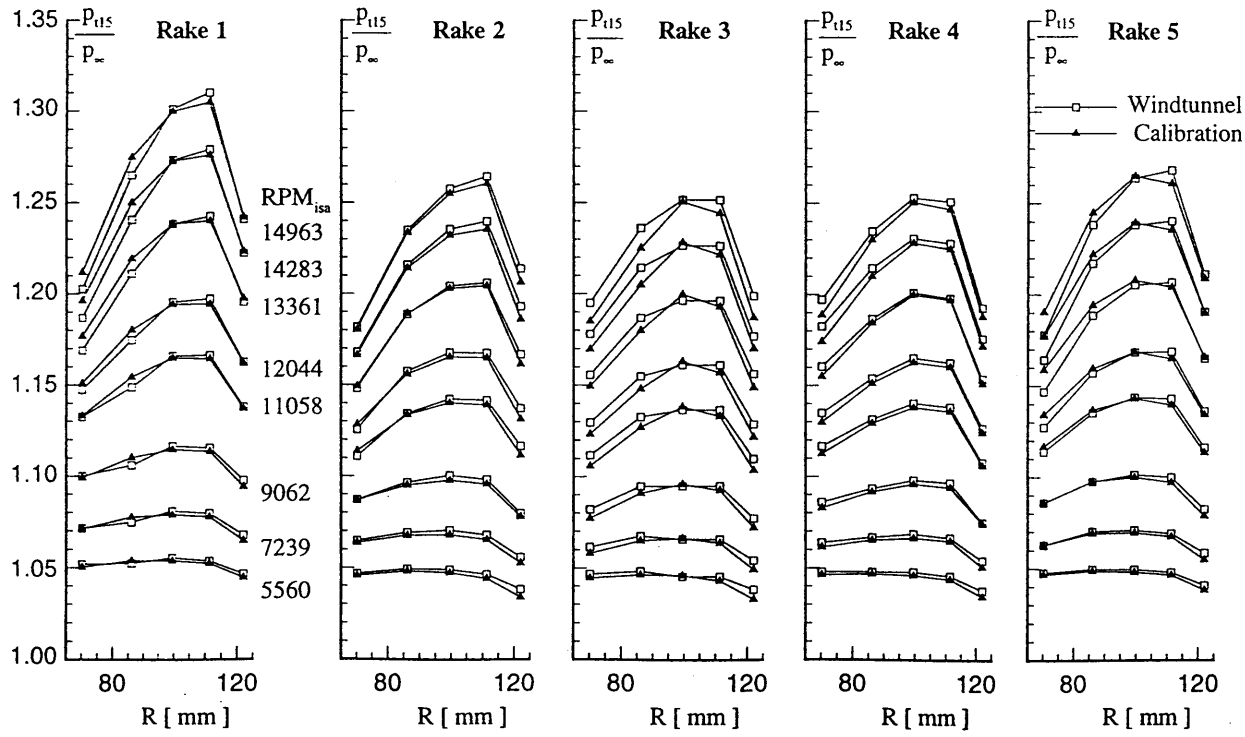

Fig. 8 Local total pressure downstream of CRUF II fan, Ma_∞=0.22, α=0°

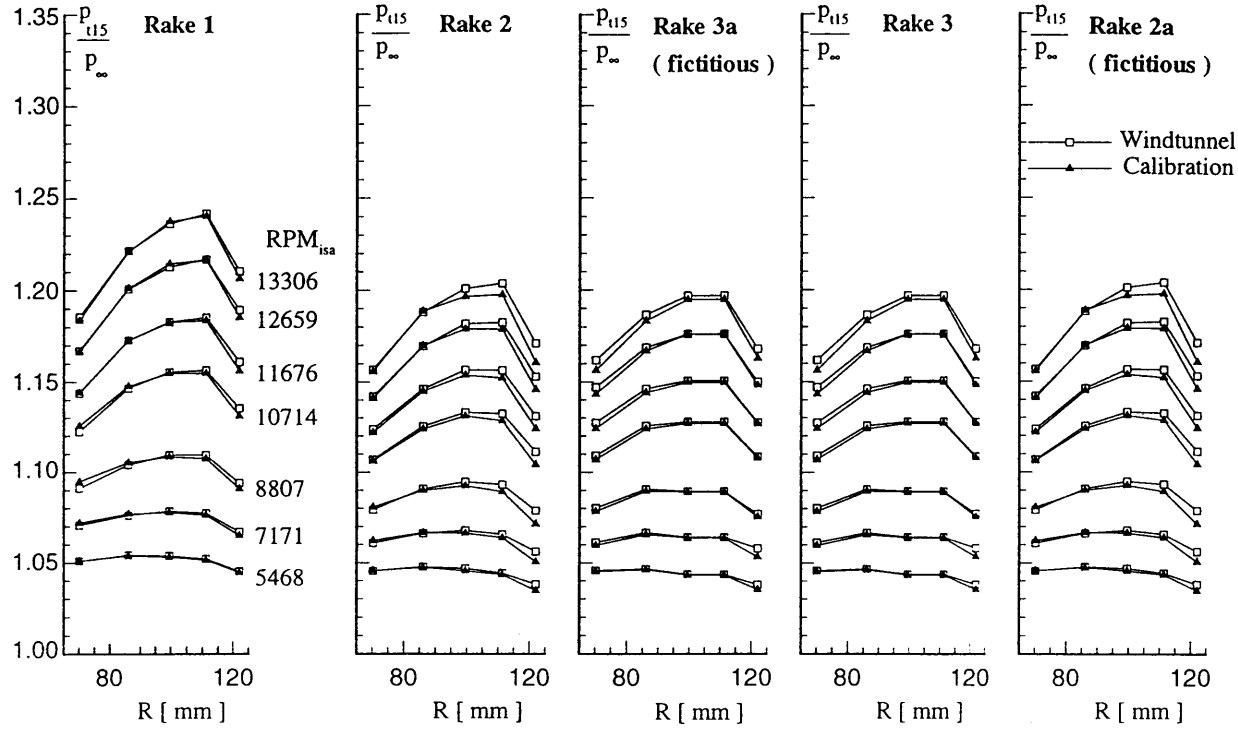

Fig. 9 Local total pressure downstream of CRUF I fan, Ma_∞=0.22, α=0°

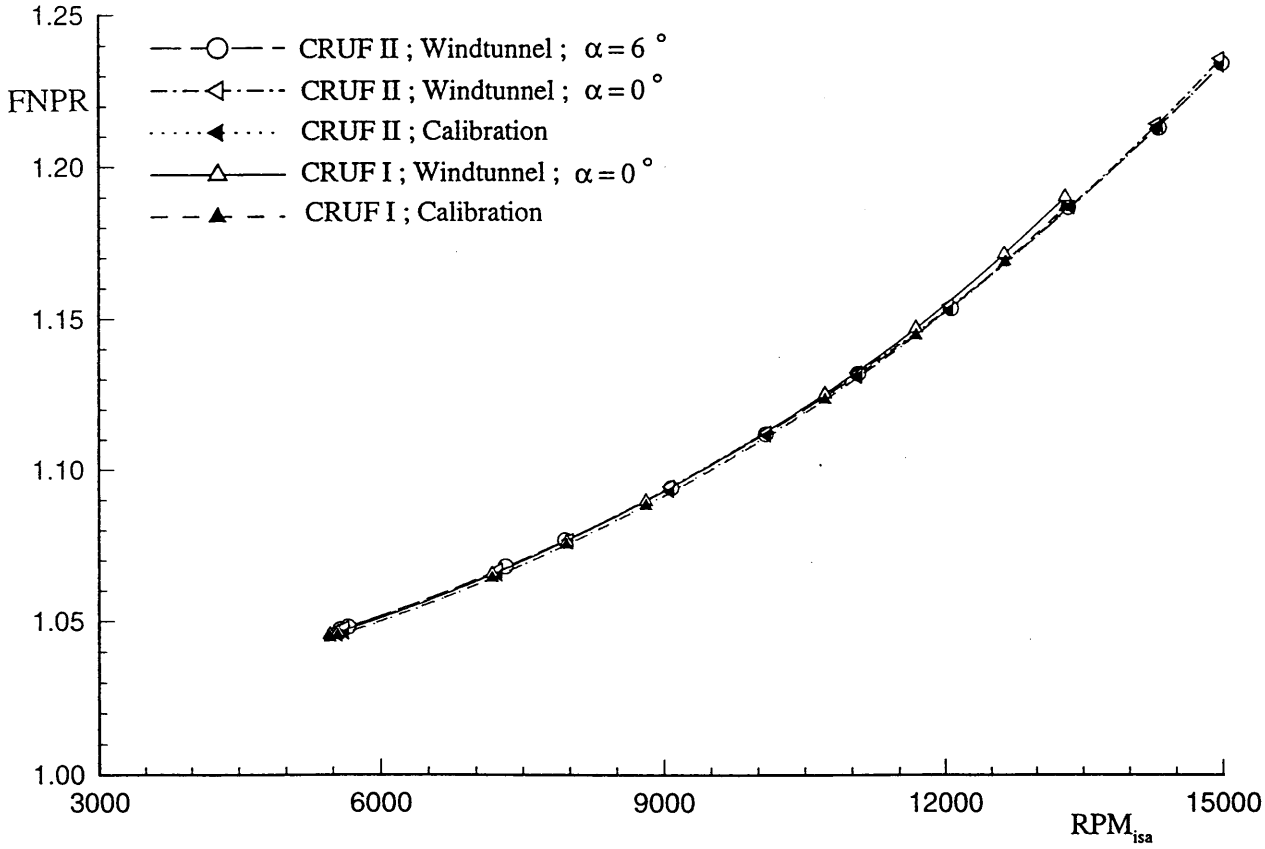

Fig. 10 Average total pressure downstream of CRUF I and II fan, Ma_∞=0.22

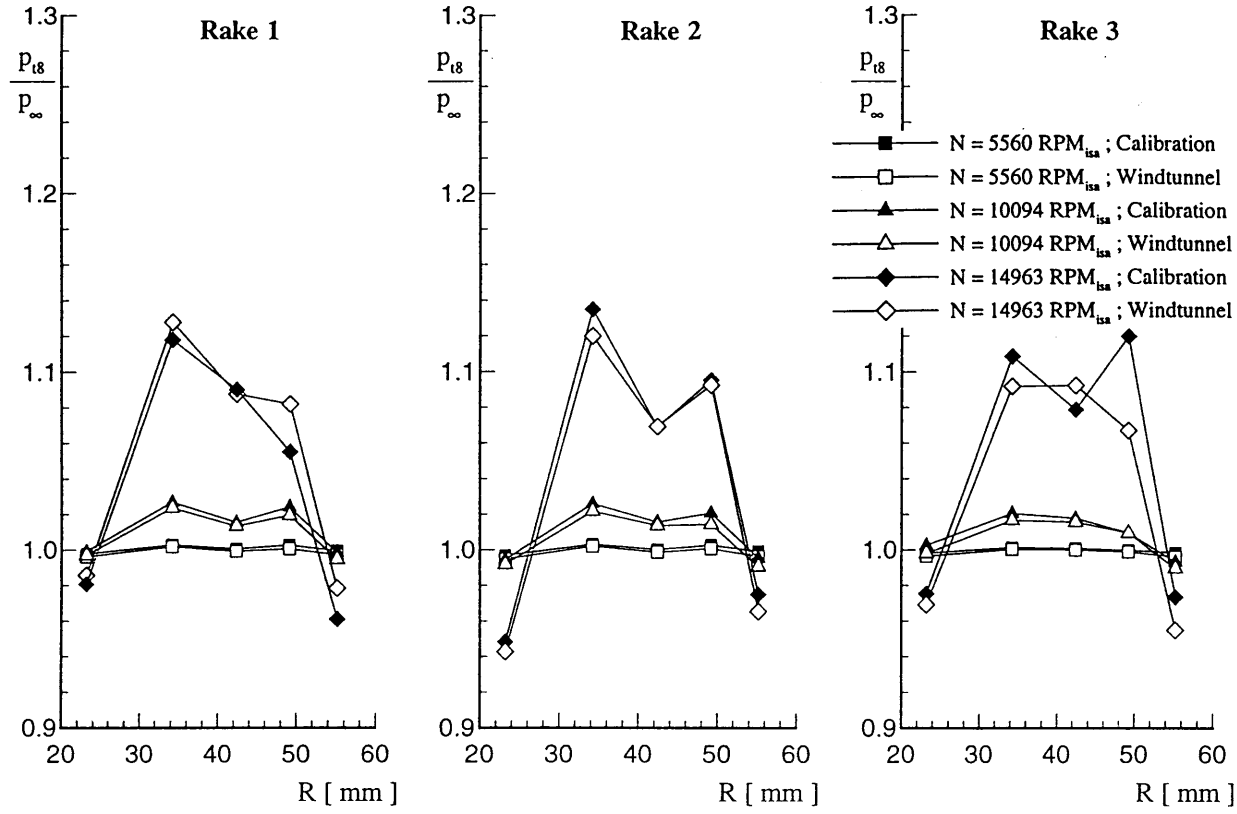

Fig. 11 Local total pressure downstream of CRUF II turbine, plane 8, Ma_∞=0.22, α=0°

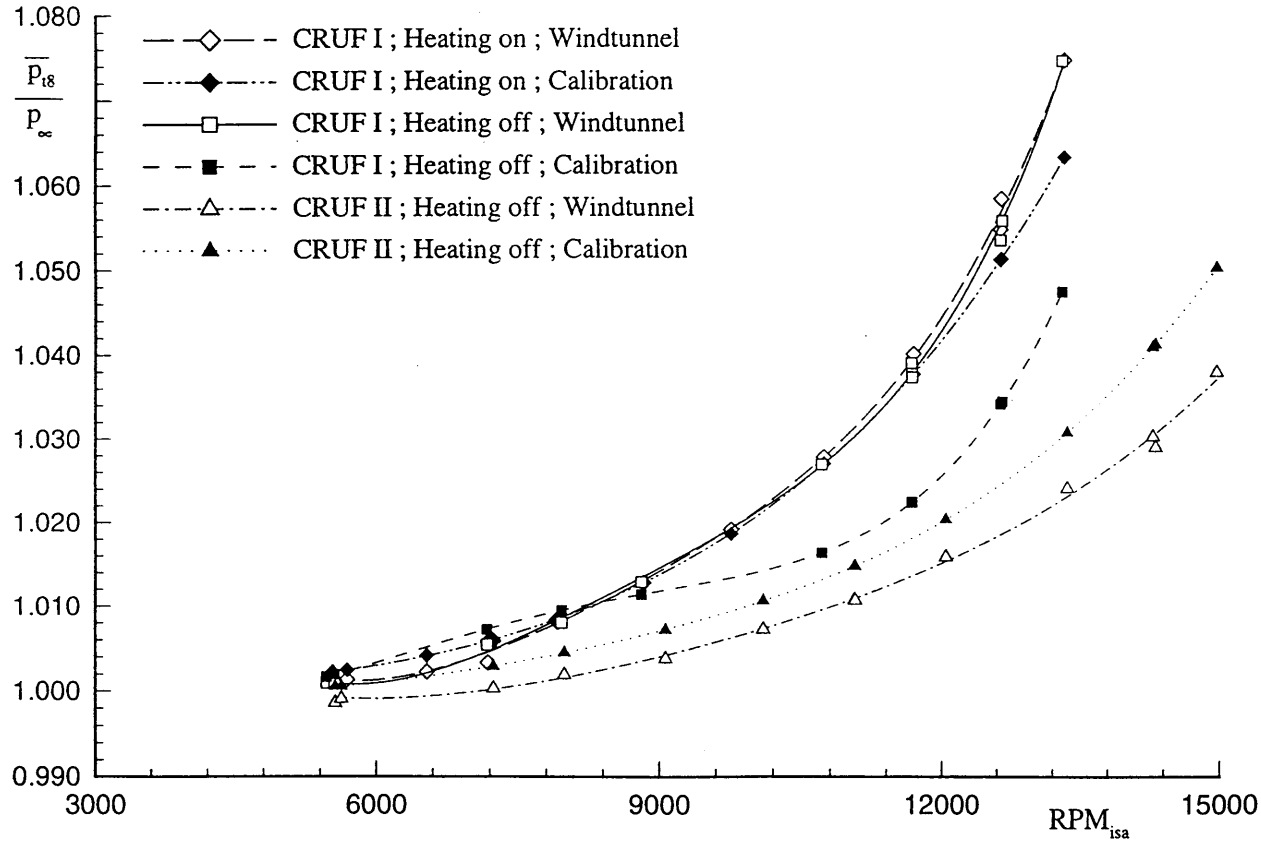

Fig. 12 Average total pressure downstream of CRUF I and II turbine, plane 8, Ma_∞=0.22, α=0°

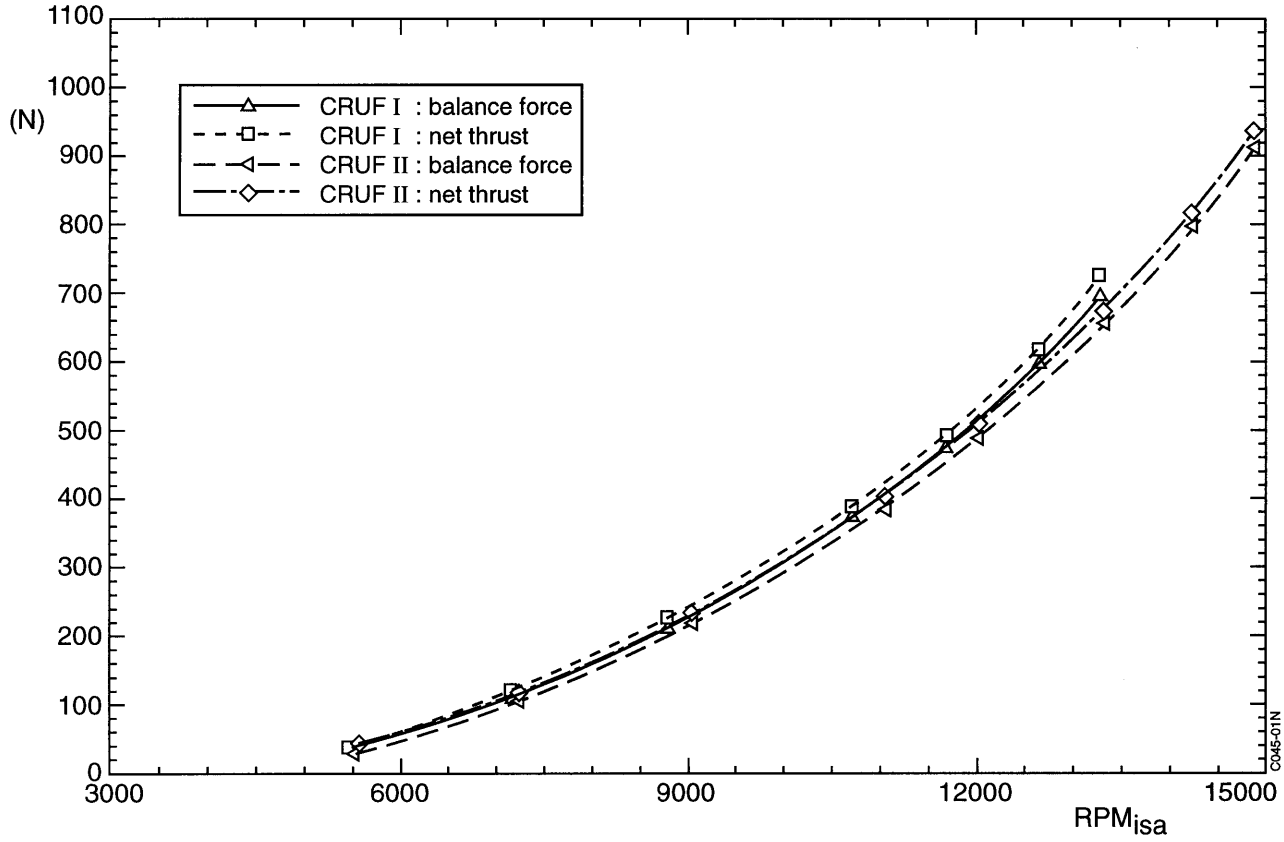

Fig. 13 Corrected Axial balance force and net thrust, plane 8, Ma_∞=0.22, α=0°

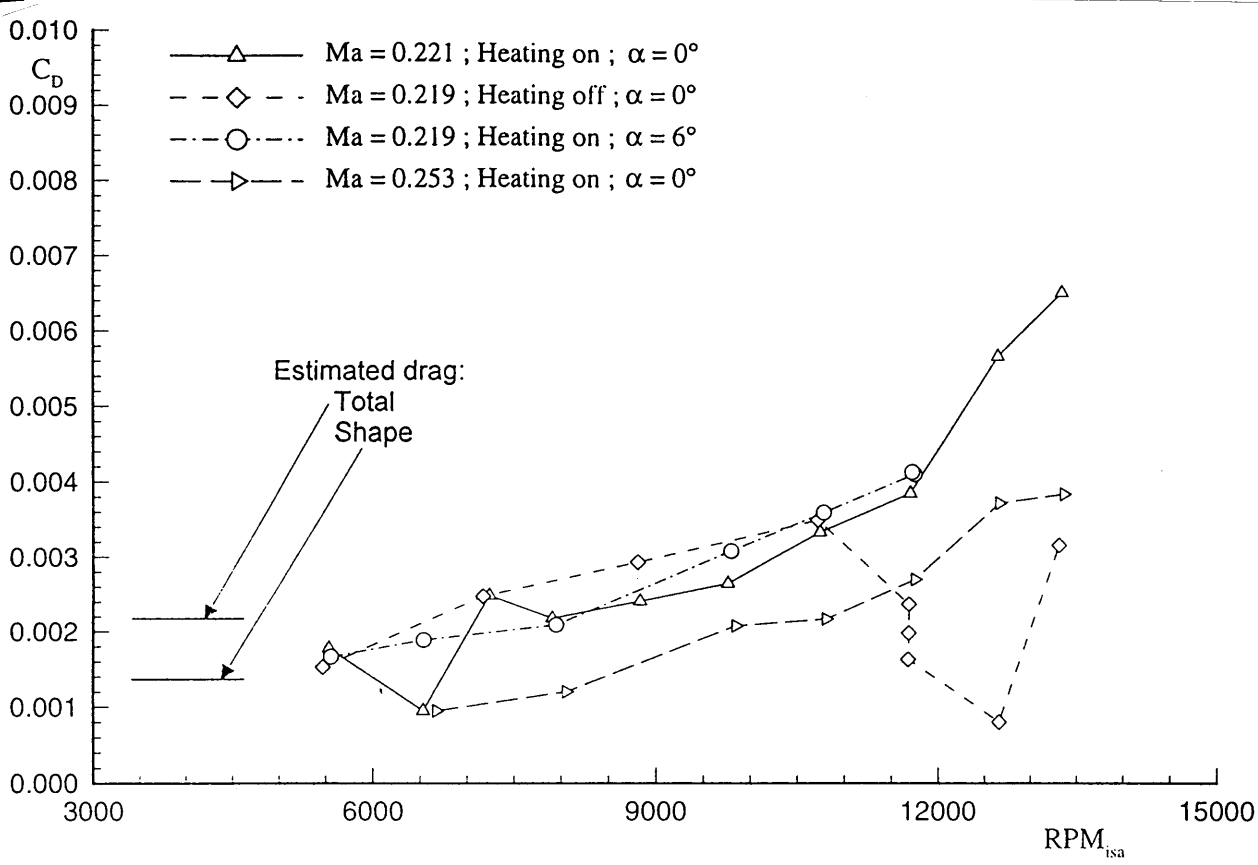

Fig. 14 Drag coefficient of CRUF I, plane 5

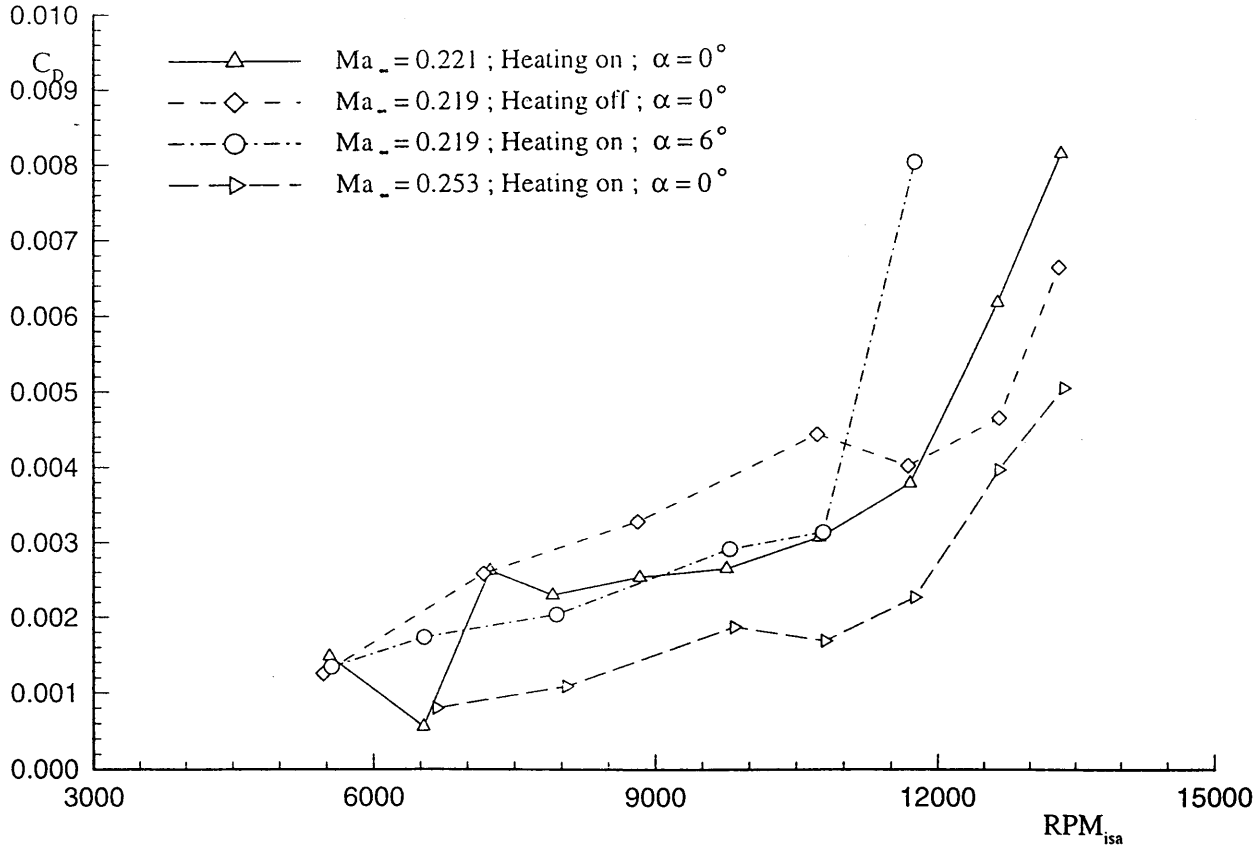

Fig. 15 Drag coefficient of CRUF I, plane 8